SUPPLEMENTARY INFORMATION for

Origin of the optical anisotropy and the electronic structures of Ru-based double perovskite oxides: DFT and XPS study

Anup Pradhan Sakhya,*[a] D. P. Rai,[b] Md. Sariful Sheikh,[a] Manabendra Mukherjee,[c] Alo Dutta[d] and T. P. Sinha[a]

[a] Department of Physics, Bose Institute, 93/1 Acharya Prafulla Chandra Road, Kolkata 700009, India.

[b] Department of Physics, Pachhunga University College, Aizawl 796001, Mizoram, India

[c] Saha Institute of Nuclear Physics, 1/AF, Bidhan Nagar, Kolkata 700 064, India

[d] Department of Condensed Matter Physics and Material Sciences, S. N. Bose National Centre for Basic Sciences, Block-JD, Sector-III, Salt Lake, Kolkata-700098.

E-mail: npshakya31@gmail.com

Phone: +91 33 23031194

S 1. COMPUTATIONAL DETAILS

The exchange correlation potential is treated by the generalized gradient approximation (GGA) as proposed by Perdew-Burke-Ernzerhof [1] in both the computational methods. We have used the simplified, rotationally invariant approach introduced by Dudarev *et al*. [2] to take into account the strong on-site Coulomb repulsion amongst the localized A 4f and Ru 4d electrons. The value of U and J used for A 4f and Ru 4d electrons are given in Table S1. Using the experimental structural parameters obtained from the Rietveld refinement of the XRD data the crystal structures have been optimized so as to minimise the forces acting on each atoms. The optimized atomic coordinates are used for further calculations and are given in Table S2**.** In this approach the valence orbital are expanded as plane waves and the interactions between the core and the valence electrons are described by pseudo potentials. The optimization of the atomic geometry is performed via conjugate-gradient minimization [3] of the total energy using Hellmann-Feynman forces on the atoms and the stresses in the unit cell. During the simulations, atomic coordinates are allowed to relax for different volumes of the unit cell. These parameters are changed iteratively so that the sum of the lattice energy and the electronic free energy are converged to a minimum value. The exact ground state for each set of atomic positions are calculated and the electronic free energy is taken as the quantity to be minimized. Convergence minimum with respect to the atomic shifts are assumed to be attained when the energy difference between the two successive iterations is less than 10^{-6} eV per unit cell and the forces acting on the atoms are less than 1 meV/Å. The plane wave cut-off energy of 500 eV and 6×6×4 *k*

mesh are used to achieve reasonable convergence. The Fermi surface was treated by the Methfessel-Paxton [4] method with a smearing of 0.5 eV. The sampling integration over the Brillouin zone is employed by using the Monkhorst-Pack method [5]. In the electronic structure calculations using spin polarized full potential linearized augmented plane wave (FP-LAPW) method as implemented in WIEN 2k, the multi-pole expansion of the crystal potential and the electron density within the muffin tin (MT) spheres are cut at *l* = 10. Muffin-tin radii (RMT) for Pr, Nd, Sm, Li, Ru and O are listed in Table S3. Non-spherical contributions to the charge density and potential within the MT spheres are considered up to l_{max} = 6. The cut-off parameter RMT×K_{max} = 7 has been chosen, which controls the convergence of the basis set (K_{max} is the plane-wave cutoff). The convergence criterion is set to be 10^{-4} Ry. The core states are treated relativistically, whereas the semi core states are treated semi-relativistically i.e. ignoring the spin-orbit (SO) coupling. The energy cut-off between the core and the valence states is set at —8.0 Ry.

Table S1. Value of U and J parameters given in eV applied to A—f and Ru—d orbitals within the GGA+U scheme.

Atom	U	J	Ref.
Pr	6.5	1.0	(6)
Nd	7.2	1.0	(6)
Sm	7.4	1.0	(6)
Ru	3.0	0.7	(7)

Table S2. Optimized atomic coordinates for A_2LiRuO_6 obtained using VASP.

PLR			
a (Å) = 5.50, b (Å)= 5.86, c (Å)=7.82, β (°) = 90.48			
Atom	x	y	z
Pr	0.016	0.931	0.749
Pr	0.984	0.069	0.251
Pr	0.484	0.431	0.751
Pr	0.516	0.569	0.249
Li	0.5	0	0
Li	0	0.5	0.5
Ru	0.5	0	0.5
Ru	0	0.5	0
O1	0.293	0.686	0.953

O1	0.707	0.314	0.047
O1	0.207	0.186	0.547
O1	0.793	0.814	0.453
O2	0.182	0.215	0.947
O2	0.818	0.785	0.053
O2	0.318	0.715	0.553
O2	0.682	0.285	0.447
O3	0.904	0.531	0.757
O3	0.096	0.469	0.243
O3	0.596	0.031	0.743
O3	0.404	0.969	0.257
NLR			
a (Å) = 5.492, b (Å)= 5.82, c (Å)=7.79, β (°) = 90.45			
Nd	0.015	0.932	0.749
Nd	0.985	0.068	0.251
Nd	0.485	0.432	0.751
Nd	0.515	0.568	0.249
Li	0.5	0	0
Li	0	0.5	0.5
Ru	0.5	0	0.5
Ru	0	0.5	0
O1	0.294	0.685	0.953
O1	0.706	0.315	0.047
O1	0.206	0.185	0.547
O1	0.794	0.815	0.453
O2	0.182	0.212	0.947
O2	0.818	0.788	0.053
O2	0.318	0.712	0.552
O2	0.682	0.288	0.447
O3	0.903	0.531	0.756
O3	0.097	0.469	0.244

O3	0.597	0.031	0.744
O3	0.403	0.969	0.256
	SLR		
	a (Å) = 5.374, b (Å)= 5.721, c (Å)=7.63, β (°) =90.56		
Sm	0.016	0.929	0.749
Sm	0.984	0.07	0.25
Sm	0.484	0.429	0.751
Sm	0.516	0.570	0.249
Li	0.5	0	0
Li	0	0.5	0.5
Ru	0.5	0	0.5
Ru	0	0.5	0
O1	0.296	0.690	0.952
O1	0.704	0.309	0.048
O1	0.204	0.190	0.548
O1	0.796	0.809	0.452
O2	0.175	0.208	0.948
O2	0.825	0.792	0.052
O2	0.325	0.708	0.552
O2	0.675	0.292	0.448
O3	0.898	0.535	0.759
O3	0.102	0.465	0.241
O3	0.602	0.035	0.741
O3	0.398	0.965	0.259

Table S3. Muffin tin radius (RMT) of A_2LiRuO_6.

Compounds	RMT (a.u.)
PLR	Pr = 2.28, Li = 1.73, Ru = 1.96, O = 1.69
NLR	Nd = 2.42, Li = 1.72, Ru = 1.96, O = 1.69
SLR	Sm = 2.39, Li = 1.74, Ru = 1.95, O = 1.68

Table S4. Structural parameters for A_2LiRuO_6 as obtained from the Rietveld analysis of XRD data.

	PLR	NLR	SLR
a (Å)	5.4623 (1)	5.4374(5)	5.3692 (1)
b (Å)	5.6873 (1)	5.7170(5)	5.7156 (1)
c (Å)	7.7329 (2)	7.7075(5)	7.6247 (2)
β (°)	90.27	90.34	90.53
Pr (4e)			
x	0.0105(5)	-0.0003(4)	0.0147(5)
y	0.9404(2)	0.9366(7)	0.9291(3)
z	0.7488(3)	0.74477(8)	0.7493(3)
Li (2d)			
(0.5,0.0,0.0)			
Ru (2c)			
(0.5,0.0,0.5)			
O_I (4e)			
x	0.304(3)	0.273(9)	0.310(3)
y	0.712(3)	0.671(9)	0.698(3)
z	0.963(7)	0.72(2)	0.956(2)
O_{II} (4e)			
x	0.201(3)	0.214(8)	0.187(3)
y	0.193(3)	0.192(9)	0.192(3)
z	0.957(3)	0.98(1)	0.957(2)
O_{III} (4e)			
x	0.909(3)	0.896(8)	0.904(3)

y	0.524(2)	0.507(7)	0.524(3)
z	0.738(2)	0.783(5)	0.741(2)
R_p	13.8	10.1	12.3
R_{wp}	17.9	12.9	17.4
R_{exp}	10.68	7.95	12.66
χ^2	2.82	2.62	1.9

Table S5. Bond lengths and bond angles for A_2LiRuO_6.

Atom	Coordination	Bond lengths (Å)	Exp.	Theory	Bond angle (°)	Exp.	Theory
PLR							
Pr	8	Ru–O_I(×2)	2.08	1.98	<Ru–O_I–Li>	153.57	148.42
Li	6	Ru–O_2(×2)	2.09	1.99	<Ru–O_2–Li>	149.89	147.54
Ru	6	Ru–O_3(×2)	2.08	1.98	<Ru–O_3–Li>	150.06	148.09
O1	5	Li–O_I(×2)	1.97	2.19			
O2	5	Li–O_2(×2)	1.99	2.19			
O3	4	Li–O_3(×2)	1.92	2.09			
NLR							
Nd	8	Ru–O_I(×2)	1.99	1.98	<Ru–O_I–Li>	161.50	148.09
Li	6	Ru–O_2(×2)	2.26	2.0	<Ru–O_2–Li>	139.9	147.09
Ru	6	Ru–O_3(×2)	1.98	1.98	<Ru–O_3–Li>	148.65	147.77
O1	5	Li–O_I(×2)	1.98	2.18			
O2	5	Li–O_2(×2)	1.97	2.17			
O3	4	Li–O_3(×2)	2.05	2.08			
SLR							
Sm	8	Ru–O_I(×2)	2.05	1.96	<Ru–O_I–Li>	148.70	148.34
Li	6	Ru–O_2(×2)	2.06	1.96	<Ru–O_2–Li>	147.76	145.71
Ru	6	Ru–O_3(×2)	2.04	1.92	<Ru–O_3–Li>	148.71	145.94
O1	5	Li–O_I(×2)	2.02	2.11			

O2	5	Li–O_2(×2)	2.03	2.14
O3	4	Li–O_3(×2)	1.92	2.06

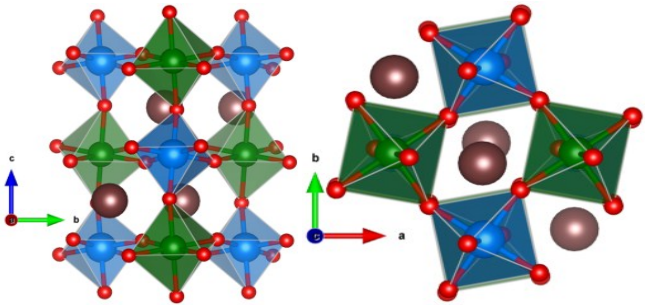

(a)

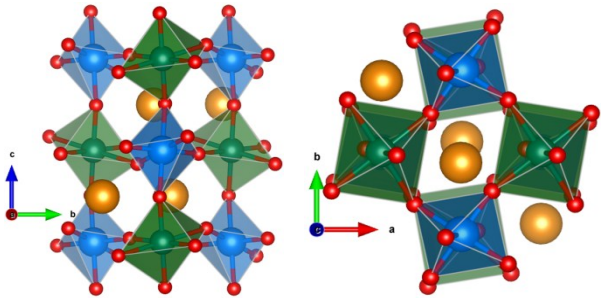

(b)

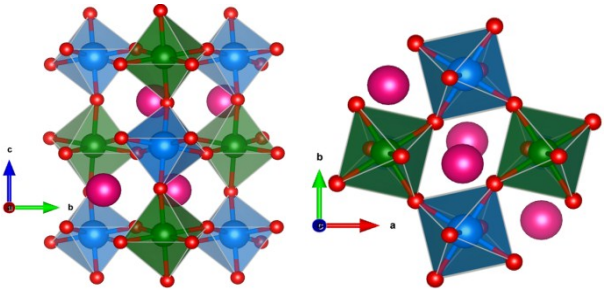

(c)

Fig. S1 Schematic presentation of the room temperature crystal structure of (a) PLR (b) NLR and (c) SLR. The blue and green colored octahedra denote the LiO_6 octahedra and RuO_6 octahedra respectively. The Pr atoms (brown spheres), Nd atoms (yellow spheres) and Sm atoms (pink spheres) sit in between the LiO_6 and RuO_6 octahedra. The Li atoms (blue spheres) and the Ru atoms (green spheres) are located at the centers of the LiO_6 and RuO_6 octahedra. The image was generated using VESTA software [8].

S 2. OPTICAL PROPERTIES

Optical properties of a solid state material indicate the interaction of the incident photon with the atoms which can be described by the dielectric function, $\varepsilon(\omega)$. The dielectric function $\varepsilon(\omega)$ of a material depending on the frequency has some important role in determining the physical properties of solids. It has two parts real and imaginary [9].

$$\varepsilon = \varepsilon_1(\omega) + i\varepsilon_2(\omega)$$

The imaginary part of the complex dielectric function can be written as

$$\varepsilon_2^{ij} = \frac{4\pi^2 e^2}{Vm^2\omega^2} \times \sum_{nn'\sigma} \langle kn\sigma \mid p_i \mid kn'\sigma\rangle\langle kn'\sigma \mid p_j \mid kn\sigma\rangle$$

$$\times f_{kn}(1 - f_{kn'})\delta(E_{kn'} - E_{kn} - \hbar\omega)$$

where e is the charge and m is the mass of the electron, the symbols ω and V represent the angular frequency of electromagnetic radiation striking the crystal, and unit cell volume respectively. $\mid kn\sigma\rangle$ represents the crystal wave function with crystal momentum k, and σ spin stands for the eigen value E_{kn} that corresponds to the momentum operator p_j. The Fermi distribution function (f_{kn}) identifies the transition from the occupied to the unoccupied state and $\delta(E_{kn'} - E_{kn} - \hbar\omega)$ shows the total energy conservation. The real part of the dielectric function $\varepsilon_1(\omega)$ can then be derived from the imaginary part using the Kramers-Kronig relation,

$$\varepsilon_1(\omega) = 1 + \frac{2}{\pi} P\int_0^\infty \frac{\omega'\varepsilon_2(\omega')}{\omega'^2 - \omega^2} d\omega'$$

where P indicates the principal value of the integral. The knowledge of both the $\varepsilon_1(\omega)$ and $\varepsilon_2(\omega)$ can be used to calculate some important optical parameters such as refractive index, reflectivity and absorption coefficients. We have calculated the dielectric function for the frequencies well above those of the phonons and therefore we have considered only the electronic excitations. Generally, in the condensed matter systems, there are two contributions to $\varepsilon(\omega)$, namely intra-band and inter-band transitions. The contribution from the intra-band transitions is important only for metals. The inter-band transitions can further be splitted into the direct and indirect transitions. The latter involve scattering of phonons and are neglected here because of their small contribution to $\varepsilon(\omega)$ in comparison to the direct transitions [10]. In order to compute the optical properties the Brillouin zone integration is performed with a dense mesh of uniformly distributed 24×17×24 k-mesh in the Brillouin zone, which corresponds to 1296 k points in the irreducible Brillouin zone.

Table S6. Optical constants of A_2LiRuO_6 compounds.

Compounds	Dielectric constant			Refractive index		Birefringence
	$\varepsilon_1^{\perp}(0)$	$\varepsilon_1^{\parallel}(0)$	$\varepsilon_1(0)$	$n^{\perp}(0)$	$n^{\parallel}(0)$	$\Delta n(0)$
PLR	5.70	5.90	5.8	2.39	2.44	0.05
NLR	5.72	5.84	5.78	2.39	2.42	0.03
SLR	5.64	5.96	5.8	2.38	2.44	0.06

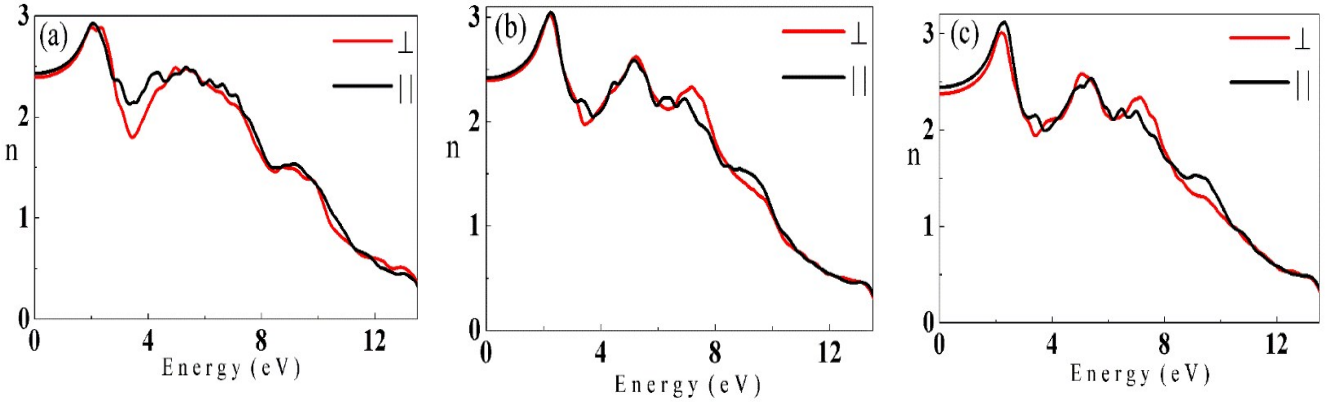

Fig. S2 Calculated refractive index (*n*) of (a) PLR, (b) NLR and (c) SLR.

S 3. Dielectric constant.

For perovskite oxides, the major contribution to the dielectric response comes from its ionic part. The ionic response is dominated by the collective effect of infrared (IR) modes and the total static dielectric tensor is expressed as:

$$\varepsilon_0^{\alpha\beta} = \varepsilon_\infty^{\alpha\beta} + \sum_\nu \varepsilon_{0,\nu}^{\alpha\beta}$$

ε_∞ is the optical dielectric tensor and $\varepsilon_{0,\nu}$ is the contribution to the dielectric constant of each individual phonon mode v. The second term is the ionic contribution to the dielectric tensor and is obtained from the following relation:

$$\varepsilon_{0,\nu}^{\alpha\beta} = \frac{4\pi e^2}{V} \sum_\nu \frac{Z_{\nu\alpha} Z_{\nu\beta}}{\omega_\nu^2}$$

where V is the volume of the unit cell, ω_ν is the eigen frequency of mode v, and $z_{\nu\beta}$ is defined as

$$Z_{\nu\beta} = \sum_{i\beta} \frac{Z_{i,\alpha\beta}^* a_{i,\nu\beta}}{\sqrt{m_i}}$$

here, m_i is the mass of the i^{th} atom, and $a_{i,\nu\beta}$ is the eigen vector of mode v.

The calculated electronic and ionic parts of static dielectric tensor for A_2LiRuO_6 are given below:

PLR = $\varepsilon_{static(electronic)} = \begin{pmatrix} 6.8 & 0.0 & 0.0 \\ 0.0 & 6.98 & 0.0 \\ 0.0 & 0.0 & 6.8 \end{pmatrix}$ $\varepsilon_{static(ionic)} = \begin{pmatrix} 21.3 & 0.0 & 0.0 \\ 0.0 & 19.7 & 0.0 \\ 0.0 & 0.0 & 16 \end{pmatrix}$

NLR = $\varepsilon_{static(electronic)} = \begin{pmatrix} 5.85 & 0.0 & 0.0 \\ 0.0 & 6.1 & 0.0 \\ 0.0 & 0.0 & 5.95 \end{pmatrix}$ $\varepsilon_{static(ionic)} = \begin{pmatrix} 30.2 & 0.0 & 0.0 \\ 0.0 & 20.0 & 0.0 \\ 0.0 & 0.0 & 19.49 \end{pmatrix}$

SLR = $\varepsilon_{static(electronic)} = \begin{pmatrix} 5.5 & 0.0 & 0.0 \\ 0.0 & 5.9 & 0.0 \\ 0.0 & 0.0 & 5.8 \end{pmatrix}$ $\varepsilon_{static(ionic)} = \begin{pmatrix} 16.5 & 0.0 & 0.0 \\ 0.0 & 17.7 & 0.0 \\ 0.0 & 0.0 & 17 \end{pmatrix}$

REFERENCES

1 J. P. Perdew, K. Burke and M. Ernzerhof, *Phys. Rev. Lett.,* 1996*,* **77**, 3865-3868.

2 S. L. Dudarev, G. A. Botton, Y. Y. Savrasov, C. J. Humphreys and A. P. Sutton, *Phys. Rev. B,* 1998, **57**, 1505-1509.

3 W. H. Press, B. P. Flannery, S. A. Teukolsky and W. T. Vetterling, *Numerical recipes: The Art of Scientific Computing,* Cambridge University Press, New York, 1986.

4 M. Methfessel and A. T. Paxton, *Phys. Rev. B,* 1989, **40**, 3616-3621.

5 H. J. Monkhorst and J. D. Pack, *Phys. Rev. B,* 1976, **13**, 5188-5192.

6 W. Setyawan and S. Curtarolo, *Comp. Mater. Sci.,* 2010, **49**, 299–312.

7 L. Seongsu, J. G. Park, D. T. Adroja, D. Khomskii, S. Streltsov, K. A. Mcewen, H. Sakai, K. Yoshimura, V. I. Anisimov, D. Mori, R. Kanno and R. Ibberson, *Nature Mater.,* 2006, **5**, 471-475.

8 K. Momma and F. Izumi, *J. Appl. Crystallogr.,* 2011, **44**, 1272-1276.

9 F. Bassani and G. P. Parravicini, *Electronic States and Optical Tansitions in Solids*, Pergamon Press Ltd., Oxford, 1975.

10 N. V. Smith, *Phys. Rev. B,* 1971, **3**, 1862-1878.